

PhotIQA: A photoacoustic image data set with image quality ratings

Anna Breger^{1,2,*} Janek Gröhl^{3,4,5} Clemens Karner²
 Thomas R Else^{3,4} Ian Selby^{6,7} Jonathan Weir-McCall^{7,8}
 Carola-Bibiane Schönlieb¹

¹University of Cambridge, DAMTP, Cambridge, United Kingdom

²Medical University of Vienna, CMPBE, Vienna, Austria

³University of Cambridge, Department of Physics, Cambridge, UK

⁴Cancer Research UK Cambridge Institute, Cambridge, UK

⁵ENI-G, a Joint Initiative of the University Medical Center Göttingen and the Max Planck Institute for Multidisciplinary Sciences, Göttingen, Germany

⁶University of Cambridge, Department of Radiology, Cambridge, UK

⁷Cambridge University Hospitals, Department of Radiology, Cambridge, UK

⁸King's College London, School of Biomedical Engineering & Imaging Sciences, London, UK

*Corresponding author. E-mail: ab2864@cam.ac.uk

1 Abstract

Image quality assessment (IQA) is crucial in the evaluation stage of novel algorithms operating on images, including traditional and machine learning based methods. Due to the lack of available quality-rated medical images, most commonly used IQA methods employing reference images (i.e. full-reference IQA) have been developed and tested for natural images. Reported application inconsistencies arising when employing such measures for medical images are not surprising, as they rely on different properties than natural images. In photoacoustic imaging (PAI), especially, standard benchmarking approaches for assessing the quality of image reconstructions are lacking. PAI is a multi-physics imaging modality, in which two inverse problems have to be solved, which makes the application of IQA measures uniquely challenging due to both, acoustic and optical, artifacts.

To support the development and testing of full- and no-reference IQA measures we assembled **PhotIQA**, a data set consisting of 1134 reconstructed photoacoustic (PA) images that were rated by 2 experts across five quality properties (overall quality, edge visibility, homogeneity, inclusion and background intensity), where the detailed rating enables usage beyond PAI. To allow full-reference assessment, highly characterised imaging test objects were used, providing a ground truth. Our baseline experiments show that HaarPSI_{med} significantly outperforms SSIM in correlating with the quality ratings (SRCC: 0.83 vs.

0.62). The dataset is publicly available at <https://doi.org/10.5281/zenodo.13325196>.

2 Background

Advances in medical imaging technologies have been groundbreaking in the last decades, including the rapid development of deep learning methods that operate on a huge amount of image data. To ensure the feasibility of a novel methodology, quantitative image quality assessment (IQA) plays an important role for quality assurance in addition to visual inspection by experts, which is often limited due to time constraints, and therefore IQA measures may even serve as the main assessment criterion. Quantitative IQA measures may be distinguished based on the required information for the assessment step [2, 22]. In full-reference (FR) IQA, a reference image is used to evaluate the quality of a corresponding (often degraded) image in a comparative way, relying on a meaningful notion of distance between the two images. In comparison, no reference (NR) IQA aims to judge the quality without a reference based on predefined properties.

Many commonly used IQA measures have been developed for natural images and tested for specific tasks on a small number of publicly available, manually rated data sets. It is unknown how well these measures expand to medical images since they have very distinct properties, and, moreover, often a different target space (color versus grayscale). Recent research has led to first insights on the applicability of common FR-IQA measures to medical imaging data, see e.g. [4, 12]. The research field suffers from the lack of publicly available image data sets with expert annotations, as well as unavailable implementations of published IQA measures. This is reflected in studies that show limitations in the design, e.g., relying on non-expert ratings (see e.g. [5]), non-realistic distortions (such as Gaussian additive noise, see e.g. [14]) or a very limited choice of IQA measures (see e.g. [18]). Combined with the scarce time resources of medical experts, there are many obstacles for the design of reproducible IQA comparison studies.

A first step to overcome these constraints is the design and sharing of realistic medical image data sets with expert quality ratings. For no-reference, recently, there have been first data sets published, see e.g. a low-dose computed tomography data set [13]. The data set PhotIQA is, to the best of our knowledge, the first publicly available, open access data set with medical images rated by experts regarding quality in the FR setting, and specifically, for PAI. Note that due to the nature of full-reference IQA, the quality ratings may also be employed to assess no-reference IQA measures when discarding the reference images.

2.1 Photoacoustic imaging and IQA

Photoacoustic imaging (PAI) is an emerging medical imaging modality with important clinical applications such as inflammatory bowel disease, cardiovascular diseases, and breast cancer [1]. It is a multi-physics modality, combining interactions of both light and sound with tissue. To reconstruct an image of the parameter of interest in PA imaging - the optical absorption coefficient - two inverse problems have to be solved: the acoustic inverse problem to reconstruct an image of absorbed energy density and the optical inverse problem of recovering optical absorption, scattering, and the Grüneisen parameter. Through limitations in the measurement hardware and non-uniqueness of absorption and scattering, both inverse problems are not trivial to solve, and PA imaging thus suffers a variety of artifacts that can significantly affect the interpretability and clinical utility of the images [7, 19].

The inverse problems of PA imaging pertain to accurately visualizing molecular distributions and determining functional tissue information from PA time series measurements [6]. It is important to identify suitable measures that can objectively assess the quality of photoacoustic image reconstructions, as finding the optimal reconstruction algorithm for the acoustic inverse problem given a certain hardware configuration is crucial for all further steps.

The state of the art is the employment of common quality measures, such as SSIM [23] or PSNR [10], which have on the other hand been shown not to be suitable [3]. Especially in PAI, with multiple possible device configurations and diverse clinical applications [15], targeted IQA measures must be developed that can accurately assess the image quality given the diagnostic parameter to be extracted from the images. The quality-rated data we present in this paper can be an important first step for initiating experiments that validate the suitability of employed IQA measures. Moreover, the provided detailed quality properties allow a comprehensive insight into task-dependent suitability. As these properties are transferable to other medical imaging tasks, the ratings can also be used for assessing the suitability of IQ measures beyond PA images.

3 Data & Methods

In this section, we will provide an overview of PhotIQA, the employed image data, and the newly obtained quality ratings.

3.1 Photoacoustic Image Data

To obtain PhotIQA, we employ a previously published open access data set, cf. [8], that consists of reconstructed PA images containing estimated distributions of the optical absorption coefficient from cross-sectional PA images of piecewise constant test objects (phantoms). The PA data were acquired with a preclinical commercial PA imaging system (MSOT InVision 256-TF, iThera Medical GmbH, Munich, Germany).

It contains 378 reference images that have been obtained using a double-integrating

sphere [16] setup as a complementary measurement system, which yields point estimates for homogeneous material samples. Because of the piecewise-constant nature of the used phantoms, one can fabricate an additional batch of the material used for the test object, measure it, and relate the calculated properties to the test object. This process is unfeasible for complicated objects or in vivo images, but can serve in this setting to obtain reference images.

By applying 3 different reconstruction methods to the time series data yielding the spatial absorption coefficient images (see Figure 1), we receive 1134 reconstructed images, each corresponding to one reference image. The reconstruction method is a two-stage approach, approximating the acoustic inverse problem with a filtered back-projection and then applying one of three methods for the optical inverse problem. These methods were recently published [8] and can be summarized as follows: *Algorithm 1* is a fluence compensation algorithm, where the reconstructed image is corrected by a Monte Carlo simulation of the light fluence. The reference absorption and scattering values are obtained through double integrating sphere reference measurements, and this approach is only feasible here through the piecewise-constant nature of the phantoms. *Algorithm 2* is a deep learning algorithm trained in a supervised fashion on purely simulated data, and *Algorithm 3* is architecturally identical to the latter, but trained on experimentally acquired data. The deep learning architecture used for this case was a U-Net, modified for a regression task. The algorithms are described in detail in the publication by Gröhl et al. [8].

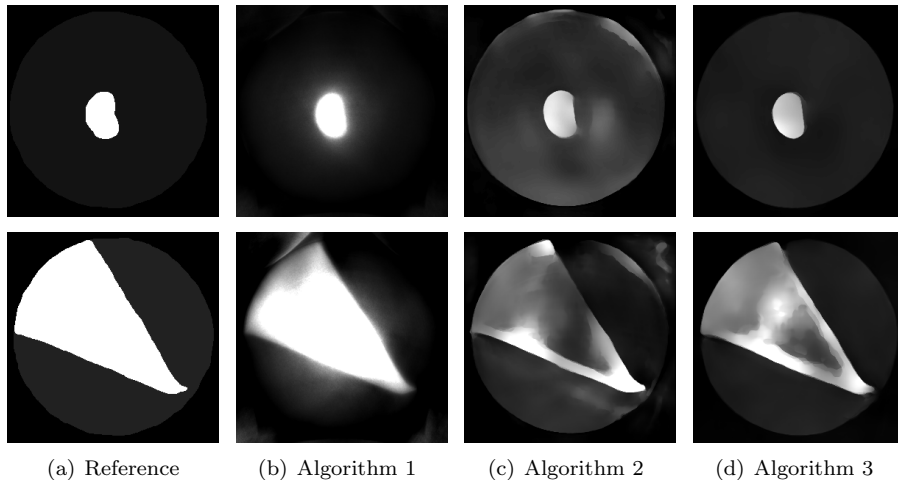


Figure 1: Two examples of images in PhotIQA, references (a) and the reconstructions from the described algorithms (b-d). Algorithm 1 (b) corrects a reconstructed PA image by using the light fluence obtained from simulations. Algorithms 2 and 3 (c-d) are deep-learning models trained to estimate the absorption coefficient.

3.2 Image Quality Ratings

Two experts have been consulted to rate the reconstructed image data described above consulting a Likert Scale, in particular, choosing 1 (very poor), 2 (poor), 3 (good) or 4 (very good) to describe the quality in comparison to the reference image. The rating was done by both experts on 2 days, taking approximately 9 hours in total. They were collected with the publicly available speedyIQA annotation app [20]. The software asks the user to set a task and the rating categories, see Figure 2. The experts were told not to change the contrast or luminance on their screen during the task. Obtained ratings have been saved in a CSV file, and to account for different rating behaviors between multiple graders, additionally, the z-score has been computed, cf. [21]. Eventually, the mean opinion scores (MOS) between the experts' ratings were computed. In the context of PhotIQA, the experts were asked to rate the images regarding

- Overall Quality,
- Edge Visibility,
- Object Homogeneity,
- Object Intensity (Inclusion Area) Intensity $_I$, and
- Object Intensity (Background) Intensity $_{BG}$.

Here, the object intensity refers to any signals arising from inside the circular test object. Inclusion areas are those areas with increased contrast, and the background refers to the base material that makes up the majority of the test object.

4 Data Records

The PA images (378 references and corresponding 1134 reconstructions) and the image quality ratings are publicly available at (<https://doi.org/10.5281/zenodo.13325196>). The original PAI image data is available via the University of Cambridge Apollo repository at (<https://doi.org/10.17863/CAM.96644>) and was published by Gröhl et al. [8].

The PA images are stored as 8-bit *png* files of size 288×288 pixels in the *zip* file "*normalised_images.zip*". The image normalization was computed by rescaling all pixel values linearly so that the minimum is mapped to 0 and the maximum to 255. This *zip* file contains the folders *./reference/*, all reference images named *"image"+#IMAGE+".png"*, and the folder *./algorithms/*, three distorted images for each reference image named *"image"+#IMAGE+"_"+#ALGORITHM+".png"* corresponding to the three employed algorithms described above.

The ratings of each quality property are stored in separate *csv* files named *"annotations_"+TASK*. These files contain the columns

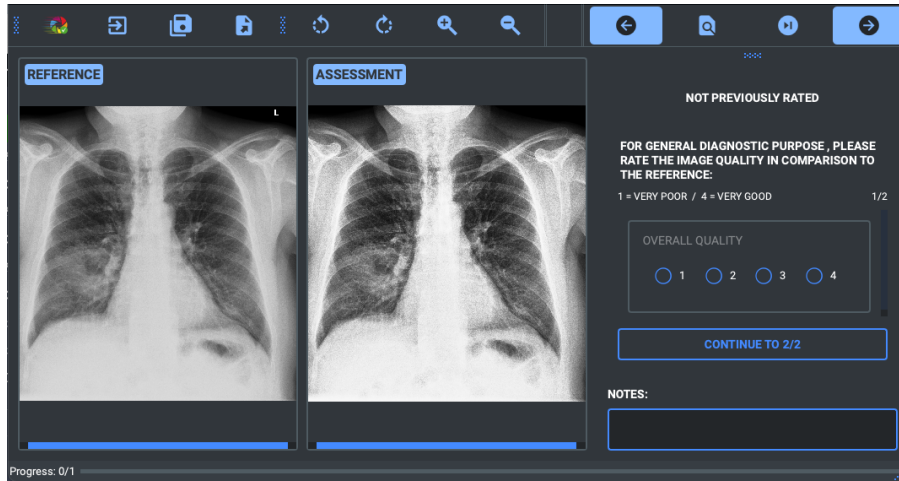


Figure 2: The speedyIQA annotation app allows setting a task and rating categories for manual image quality ratings.

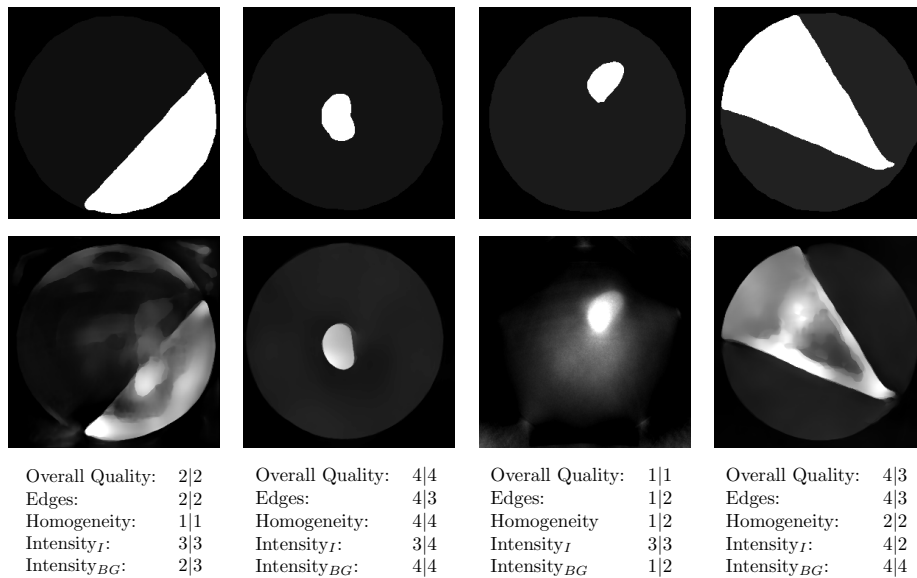


Figure 3: Four examples of quality ratings from both annotators for the different detailed quality properties. (Top) reference image and (bottom) reconstructed, assessed image.

- "filename": File name of the distorted image file
- TASK+"_1": Ratings from the first expert
- TASK+"_2": Ratings from the second expert

- TASK+”_mos”: MOS of both ratings
- TASK+”_zscore_mos”: MOS of the z-scores of both ratings

5 Technical Validation

5.1 Inter-rater consistency

First, we study the IQA ratings provided by the experts. In Figure 4 we verify the agreement of ratings between the two experts. We show here the box plot of the absolute differences between the raters, once for the raw data and once for the z-scores. We can see directly that the absolute difference of the raw ratings is at most 0.5 and the median equals 0 for all quality properties, indicating that at least half of the ratings are identical for both experts. The z-scores compensate for biases of individual raters towards low or high scores that may limit the direct interpretability. For example, the meaning of the rating (4) might differ between both experts depending on a tendency towards low or high ratings, and the z-scores allow insights into the corrected difference. In the box plot corresponding to the z-scores, we can observe that the highest agreement was achieved for the properties “Homogeneity” and “Intensity (Inclusion)” with a median close to 0. The strongest disagreement was identified within the category “Overall Quality” and the most outliers were in the category “Edges”. Visual examples of the extreme outliers in the categories “Overall Quality” and “Edges” are provided in Figure 6.

Moreover, in Figure 5 we show the amount of each rating given per task. We observe that the rating (1) was given much less than the ratings (2-4), which is caused by the reconstructed images stemming from three reconstruction algorithms that all give somewhat reasonable results. The property intensity (inclusion area) received mostly the highest ratings. The other properties show behavior closer to a normal distribution peaking at the rating (3). Rater 2 showed a different rating behavior regarding (4), which they used much less than rater 1, where the z-score accounts for that.

5.2 IQA evaluation

To give a baseline assessment of the validity of common IQA measures, we compare their values to the manual ratings. The chosen IQA measures were computed with default implementations provided by their authors, either in MATLAB or Python. For the evaluation of the IQ measures’ performance, we employ the Spearman Rank Correlation Coefficient (SRCC) and the Kendall Rank Correlation Coefficient (KRCC), which assess the rank between the IQA measures and the manual ratings. The absolute SRCC and KRCC between the MOS of the z-scores and the IQA measures are stated in Table 1. We can observe that HaarPSI, especially in the HaarPSI_{med} [11] setting, yields good results in all categories, whereas the commonly used measures PSNR and SSIM struggle for almost all quality properties. As expected exception, PSNR is the best measure

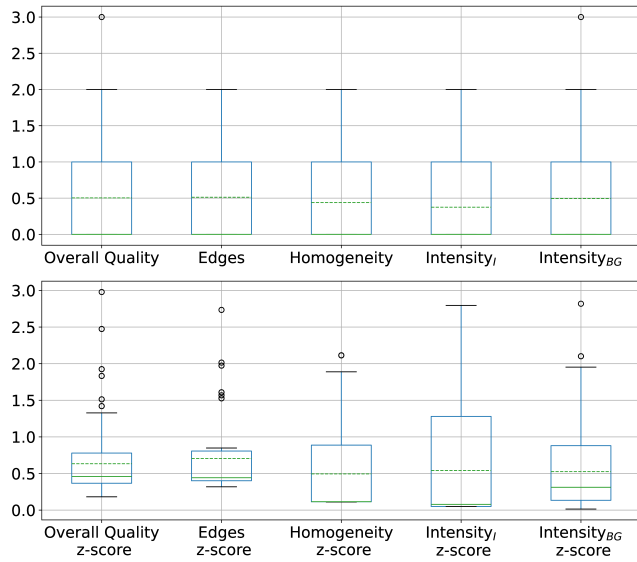


Figure 4: Box plot of the absolute differences (top) and the absolute differences of z-scores (bottom) of both raters with the median (green line) and mean (striped green line).

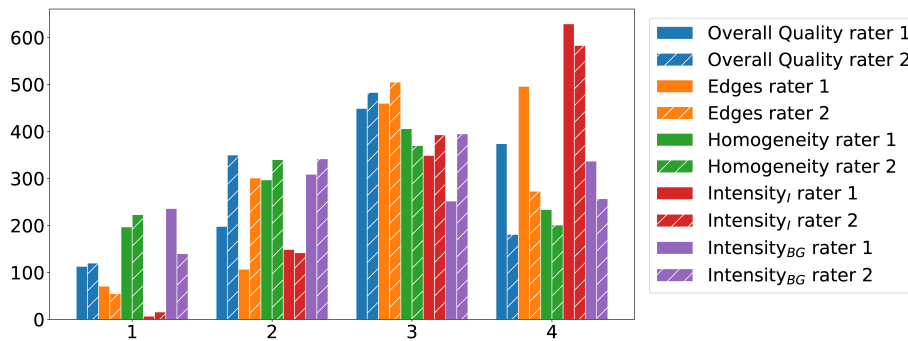


Figure 5: The distribution of the ratings given by both experts for all quality properties.

regarding the intensity values, as it directly computes the pixel-wise difference. In line with previous experiments, besides HaarPSI [17], MS-SSIM [27], IW-SSIM [24], LPIPS [26], and GMSD [25] show promising behaviors.

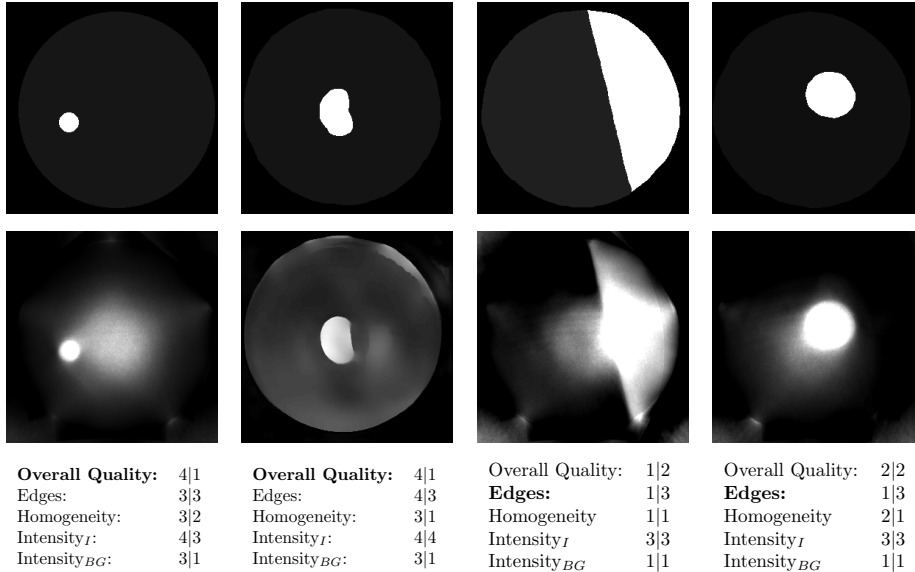


Figure 6: Four examples of rating disagreements corresponding to box plot outliers in Figure 4(properties in bold). Reference image (top) and reconstructed, assessed image (bottom).

6 Usage notes

In order to pair the images with the scores of a specific property, e.g. overall quality, we employ the *csv* file *"annotations_overall_quality.csv"*. The filename leads to the corresponding *png* images in the folders *"./algorithms/"* and *"./references/"* contained in the *zip* file *"normalised_images.zip"*.

6.1 Limitations

The ratings were obtained by just 2 experts, which does not reflect a large and diverse cohort of raters. Nevertheless, we have seen in Section 5 that their ratings do agree on the majority of data whilst both raters showed individual behavior regarding scoring.

The two-stage PA reconstruction was done using filtered back-projection for the acoustic inverse problem. While we expect a deep learning based approach for the optical inversion to learn to account for systematic reconstruction artifacts, the concrete algorithm for the acoustic inversion is expected to have an impact [9]. Moreover, in this work, we evaluate the PAI reconstruction performance purely on the bases of comparing reconstructed absorption coefficients to reference absorption coefficients. In a clinical setting, this might not always be the most important endpoint and it may already be sufficient to reconstruct relative multispectral signal responses to gain access to relative molecular concentration differences. Furthermore, the narrow endpoint limits the spectrum

	Overall Quality	Edges	Homogeneity	Intensity _I	Intensity _{BG}
PSNR*	0.71/0.54	0.63/0.47	0.75/0.57	0.68/0.53	0.61/0.46
SSIM*	0.62/0.48	0.64/0.49	0.62/0.46	0.40/0.30	0.66/0.50
HaarPSI _{med}	0.83/0.68	0.80/0.64	0.80/0.63	0.55/0.40	0.81/0.64
HaarPSI	0.81/0.65	0.77/0.60	0.78/0.61	0.57/0.42	0.77/0.60
MS-SSIM	0.81/0.65	0.75/0.60	0.83/0.67	0.55/0.41	0.81/0.64
IW-SSIM*	0.79/0.63	0.75/0.59	0.80/0.64	0.59/0.44	0.80/0.62
GMSD*	0.77/0.60	0.68/0.52	0.80/0.63	0.62/0.47	0.71/0.55
FSIM*	0.78/0.62	0.72/0.56	0.80/0.63	0.58/0.44	0.76/0.59
MDSI*	0.68/0.51	0.63/0.48	0.69/0.51	0.61/0.46	0.59/0.43
LPIPS _{Alex}	0.76/0.59	0.78/0.63	0.73/0.56	0.43/0.31	0.79/0.61
DISTS*	0.70/0.56	0.69/0.54	0.74/0.58	0.42/0.31	0.77/0.60
NIQE*	0.53/0.39	0.40/0.28	0.65/0.49	0.48/0.36	0.53/0.39
PAQ2PIQ	0.20/0.14	0.28/0.20	0.07/0.06	0.07/0.04	0.30/0.21

Table 1: Baseline results: SRCC/KRCC between the MOS of the manual expert ratings’ z-scores and common full-reference (top) and no-reference (bottom) IQA measures. * denotes that implementations were provided in MATLAB. The 3 highest results are bold.

of PAI artifacts represented by this dataset. In this work, we only look at three reconstruction algorithms (one physics-based, two deep learning variants), and the results we find may not generalize to all PAI tasks.

Lastly, the chosen quality properties leave room for subjective interpretation. Nonetheless, we argue that this is not exceeding expected behavior when dealing with tasks that are not analytically quantifiable.

7 Code Availability

The code for the PAI reconstruction algorithms is available open source at (https://github.com/BohndiekLab/end_to_end_phantom_QPAT). The Python code of the IQA experiments, including the implementations of the Python based IQA measures, is available on GitHub <https://github.com/ideal-iqa/iqa-eval>. The speedyIQA annotation app is available at https://github.com/selbs/speedy_iqa.

References

- [1] Assi, H., Cao, R., et al: A review of a strategic roadmapping exercise to advance clinical translation of photoacoustic imaging: From current barriers to future adoption. *Photoacoustics* **32**, 100539 (2023). <https://doi.org/https://doi.org/10.1016/j.pacs.2023.100539>
- [2] Athar, S., Wang, Z.: A comprehensive performance evaluation of image quality assessment algorithms. *IEEE Access* **7**, 140030–140070 (09 2019). <https://doi.org/10.1109/ACCESS.2019.2943319>

- [3] Breger, A., Biguri, A., Landman, M.S., Selby, I., Amberg, N., Brunner, E., Gröhl, J., Hatamikia, S., Karner, C., Ning, L., Dittmer, S., Roberts, M., Schönlieb, C.B., Collaboration, A.C.: A study of why we need to reassess full reference image quality assessment with medical images. *Journal of Imaging Informatics in Medicine* (2025). <https://doi.org/10.1007/s10278-025-01462-1>, <https://doi.org/10.1007/s10278-025-01462-1>
- [4] Breger, A., Karner, C., Selby, I., Gröhl, J., Dittmer, S., Lilley, E., Babar, J., Beckford, J., Sadler, T.J., Shahipasand, S., Thavakumar, A., Roberts, M., Schönlieb, C.B.: A study on the adequacy of common iqa measures for medical images. In: *Proceedings of 2024 International Conference on Medical Imaging and Computer-Aided Diagnosis (MICAD)*, Springer Lecture Notes in Electrical Engineering (2024)
- [5] Chow, L.S., Rajagopal, H., Paramesran, R.: Correlation between subjective and objective assessment of magnetic resonance (mr) images. *Magn Reson Imaging* **34**(6), 820–831 (Jul 2016). <https://doi.org/10.1016/j.mri.2016.03.006>
- [6] Cox, B., Laufer, J.G., Arridge, S.R., Beard, P.C.: Quantitative spectroscopic photoacoustic imaging: a review. *J Biomed Opt* **17**(6), 061202 (Jun 2012). <https://doi.org/10.1117/1.JBO.17.6.061202>
- [7] Else, T.R., Loreno, C., Groves, A., Cox, B.T., Gröhl, J., Modolell, I., Bohndiek, S.E., Roshan, A.: The confounding effects of skin colour in photoacoustic imaging. *medRxiv* pp. 2025–03 (2025)
- [8] Gröhl, J., Else, T.R., Hacker, L., Bunce, E.V., Sweeney, P.W., Bohndiek, S.E.: Moving beyond simulation: data-driven quantitative photoacoustic imaging using tissue-mimicking phantoms. *IEEE Trans Med Imaging* **PP** (Nov 2023). <https://doi.org/10.1109/TMI.2023.3331198>
- [9] Gröhl, J., Kunyansky, L., Poimala, J., Else, T.R., Di Cecio, F., Bohndiek, S.E., Cox, B.T., Hauptmann, A.: Digital twins enable full-reference quality assessment of photoacoustic image reconstructions. *arXiv preprint arXiv:2505.24514* (2025)
- [10] Gröhl, J., Schellenberg, M., Dreher, K., Maier-Hein, L.: Deep learning for biomedical photoacoustic imaging: A review. *Photoacoustics* **22**, 100241 (2021)
- [11] Karner, C., Gröhl, J., Selby, I., Babar, J., Beckford, J., Else, T.R., Sadler, T.J., Shahipasand, S., Thavakumar, A., Roberts, M., Rudd, J.H., Schönlieb, C.B., Weir-McCall, J.R., Breger, A.: Parameter choices in haarpsi for iqa with medical images. In: *2025 IEEE 22nd International Symposium on Biomedical Imaging (ISBI)*. pp. 1–5 (2025). <https://doi.org/10.1109/ISBI60581.2025.10981227>
- [12] Kastrulin, S., Zakirov, J., Pezzotti, N., Dylvov, D.V.: Image quality assessment for magnetic resonance imaging. *IEEE Access* **11**, 14154–14168 (2023). <https://doi.org/10.1109/ACCESS.2023.3243466>
- [13] Lee, W., Wagner, F., Galdran, A., Shi, Y., Xia, W., Wang, G., Mou, X., Ahamed, M.A., Imran, A.A.Z., Oh, J.E., Kim, K., Baek, J.T., Lee, D., Hong, B., Tempelman, P., Lyu, D., Kuiper, A., van Blokland, L., Calisto, M.B., Hsieh, S., Han, M., Baek, J., Maier, A., Wang, A., Gold, G.E., Choi, J.H.: Low-dose computed tomography perceptual image quality assessment. *Medical Image Analysis* **99**, 103343 (2025). <https://doi.org/https://doi.org/10.1016/j.media.2024.103343>, <https://www.sciencedirect.com/science/article/pii/S1361841524002688>

- [14] Ohashi, K., Nagatani, Y., Yoshigoe, M., Iwai, K., Tsuchiya, K., Hino, A., Kida, Y., Yamazaki, A., Ishida, T.: Applicability evaluation of full-reference image quality assessment methods for computed tomography images. *Journal of Digital Imaging* **36**(6), 2623–2634 (2023). <https://doi.org/10.1007/s10278-023-00875-0>
- [15] Park, J., Choi, S., Knieling, F., Clingman, B., Bohndiek, S., Wang, L.V., Kim, C.: Clinical translation of photoacoustic imaging. *Nature Reviews Bioengineering* **3**(3), 193–212 (Mar 2025). <https://doi.org/10.1038/s44222-024-00240-y>
- [16] Pickering, J.W., Prahl, S.A., van Wieringen, N., Beek, J.F., Sterenborg, H.J.C.M., van Gemert, M.J.C.: Double-integrating-sphere system for measuring the optical properties of tissue. *Appl. Opt.* **32**(4), 399–410 (Feb 1993). <https://doi.org/10.1364/AO.32.000399>
- [17] Reisenhofer, R., Bosse, S., Kutyniok, G., Wiegand, T.: A haar wavelet-based perceptual similarity index for image quality assessment. *Signal Process. Image Commun.* **61**, 33–43 (2018). <https://doi.org/10.1016/j.image.2017.11.001>
- [18] Renieblas, G.P., Nogués, A.T., González, A.M., Gómez-Leon, N., Del Castillo, E.G.: Structural similarity index family for image quality assessment in radiological images. *J Med Imaging (Bellingham)* **4**(3), 035501 (Jul 2017). <https://doi.org/10.1117/1.JMI.4.3.035501>
- [19] Rietberg, M.T., Gröhl, J., Else, T.R., Bohndiek, S.E., Manohar, S., Cox, B.T.: Artifacts in photoacoustic imaging: Origins and mitigations. *arXiv preprint arXiv:2504.12772* (2025)
- [20] Selby, I.: Github repository speedyiq (March 2024), https://github.com/selbs/speedy_iqa
- [21] Sheikh, H., Sabir, M., Bovik, A.: A statistical evaluation of recent full reference image quality assessment algorithms. *IEEE Transactions on Image Processing* **15**(11), 3440–3451 (2006). <https://doi.org/10.1109/TIP.2006.881959>
- [22] Wang, Z., Bovik, A., Sheikh, H., Simoncelli, E.: Image quality assessment: from error visibility to structural similarity. *IEEE Transactions on Image Processing* **13**(4), 600–612 (2004). <https://doi.org/10.1109/TIP.2003.819861>
- [23] Wang, Z., Bovik, A., Sheikh, H., Simoncelli, E.: Image quality assessment: from error visibility to structural similarity. *IEEE Transactions on Image Processing* **13**(4), 600–612 (2004). <https://doi.org/10.1109/TIP.2003.819861>
- [24] Wang, Z., Li, Q.: Information content weighting for perceptual image quality assessment. *IEEE Transactions on Image Processing* **20**(5), 1185–1198 (2011). <https://doi.org/10.1109/TIP.2010.2092435>
- [25] Xue, W., Zhang, L., Mou, X., Bovik, A.C.: Gradient magnitude similarity deviation: A highly efficient perceptual image quality index. *IEEE Transactions on Image Processing* **23**(2), 684–695 (2014). <https://doi.org/10.1109/TIP.2013.2293423>
- [26] Zhang, R., Isola, P., Efros, A.A., Shechtman, E., Wang, O.: The unreasonable effectiveness of deep features as a perceptual metric. In: *2018 IEEE/CVF Conference on Computer Vision and Pattern Recognition*. pp. 586–595 (2018). <https://doi.org/10.1109/CVPR.2018.00068>
- [27] Zhou Wang, E.P.S., Bovik, A.C.: Multi-scale structural similarity for image quality assessment. In: *Proceedings of the 37th IEEE Asilomar Conference on Signals, Systems and Computers*, Pacific Grove, CA (2003)